2014

One-sample Bayes inference for symmetric distributions of 3-D rotations

Yu Qiu
Iowa State University, yuqiu@iastate.edu

Danial J. Nordman
Iowa State University, dnordman@iastate.edu

Stephen B. Vardeman
Iowa State University, vardeman@iastate.edu

One-Sample Bayes Inference for Existing Symmetric Distributions on 3-D Rotations

YU QIU, DANIEL J. NORDMAN

Department of Statistics, Iowa State University

yuqiu@iastate.edu dnordman@iastate.edu

STEPHEN B. VARDEMAN

Department of Statistics, Department of Industrial and Manufacturing Systems Engineering, Iowa State University

vardeman@iastate.edu

Abstract

We consider a variety of existing symmetric parametric models for 3-D rotations found in both statistical and materials science literatures, from the point of view of the "uniform-axis-random-spin" (UARS) construction. We provide one-sample Bayes methods with non-informative priors for all of these models and establish attractive frequentist properties for Bayes inference on the model parameters. Taken together with earlier work of Bingham et al. (2009b), Bingham et al. (2010), and

This is a manuscript of an article published as One-sample Bayes inference for existing symmetric distributions on 3-d rotations. Computational Statistics and Data Analysis, 2014, Vol. 71, pp. 520-529, DOI:10.1016/j.csda.2013.02.004. With Yu Qiu and Dan Nordman.

Yu et al. (2012), the present work establishes conclusively the broad efficacy of non-informative Bayes inference for symmetric distributions on 3-D rotations.

Key words: Convergence Rate; Coverage Rate; Jeffreys Prior; MCMC; UARS Class

1 INTRODUCTION

This paper concerns statistical analysis for orientations in three dimensions as represented by 3×3 rotation matrices. Probability models for 3-D orientations are used in many application areas including crystallography and quantitative texture analysis in materials science. There, variation in orientation of crystal structures across a specimen is related to macro-level physical properties of a material. Symmetric distributions have been of most interest in materials applications.

Bingham et al. (2009a) studied the "uniform-axis-random-spin" (UARS) class of 3-D rotations as directionally symmetric random rotational perturbations around some "central" orientation, and Hielscher et al. (2010) identified the same class. The UARS class has a simple, physically motivated construction and directly interpretable parameters. A UARS distribution has a central location parameter $\mathbf{S}$ and a concentration parameter κ for some symmetric 2-D angular distribution with density $C(\cdot|\kappa)$ on $(-\pi, \pi]$ governing a spin of $\mathbf{S}$ around an independent uniformly distributed axis. UARS distributions ap-

pearing in the statistical and materials science literatures include the von-Mises (vM) UARS distribution (Bingham et al. 2009b), the symmetric Matrix Fisher distribution (Downs, 1972), the Lorentzian distribution (Matthies, 1982), Bunge's Gaussian distribution (Bunge, 1982), the rotational normal distribution (Matthies,1988) (i.e., the isotropic Gaussian distribution (Savjolova, 1985)), the de la Vallée Poussin distribution (Schaeben, 1997)(i.e., the Cayley distribution (León et al. 2006)), and the wrapped Maxwell-Boltzman (wMB) UARS distribution (Yu et al. 2012). All these distributions have the UARS structure with different choices of angular distributions.

Most existing works for distributions on rotations focus on likelihood-based inference and moment estimation (see for example Jupp et al. 1979, Chang et al. 2001, Rivest et al. 2006, Oualkacha et al. 2008) and consider large sample properties. Often large sample estimation results do not provide easily interpretable (in terms of their geometry) confidence regions for the parameter $\mathbf{S}$, and therefore do not clearly convey information about statistical precision. In contrast, the Bayes methods presented in this paper provide credible regions for $\mathbf{S}$ which not only have a simple geometrical structure indicating precision, but also frequentist coverage properties matching the credible levels.

In this paper we explore one-sample Bayes inference for the two parameters of all UARS distributions that have appeared in the literature plus that for a new wrapped normal (wN) UARS distribution. In Section 2, we first review the forms of all published UARS distributions and identify non-informative priors for the location and concentration parameters. In Section 3, we identify the corresponding posterior distributions and we summarize a general MCMC

algorithm for sampling from the posteriors. We then briefly describe the construction of cone-based confidence regions for location parameters. In Section 4, a simulation study for one-sample Bayes inferences is provided in order to establish the frequentist properties for the Bayes methods in all UARS models. Section 5 summarizes and suggests future work.

2 Models and Priors for the Parameters

Before listing the models in the UARS class that have been studied in the literature, it is worthwhile to reiterate the general expression for an orientation density function (ODF) in the UARS class. Given an angular density $C(r|\kappa)$, defined on $(-\pi, \pi]$ and symmetric about zero with concentration parameter κ, and a central orientation parameter $\mathbf{S} \in SO(3)$ (the set of 3×3 orthogonal matrices with determinant 1), a UARS observation $\mathbf{O}$ has a density with respect to the Haar measure (uniform distribution) on the set of rotations of the form

$$f(\mathbf{o}|\mathbf{S}, \kappa) = \frac{4\pi}{3 - tr(\mathbf{S}^T\mathbf{o})} C(\arccos[2^{-1}(tr(\mathbf{S}^T\mathbf{o}) - 1)]|\kappa), \quad \mathbf{o} \in SO(3) \qquad (1)$$

where $tr(\cdot)$ and $(\cdot)^T$ denote respectively the matrix trace and transpose; see Bingham et al. (2009a) for details.

For Bayes inference, we must first find appropriate priors for the model parameters. Following the approach of Bingham et al. (2009b), we use the uniform distribution on $SO(3)$ (which has the ODF $p(\mathbf{S}) = 1$ corresponding

to an angular density $C(r) = \frac{1-\cos(r)}{2\pi}$ in (1) for $r \in (-\pi, \pi]$) as the prior for the location parameter, $\mathbf{S}$, and adopt (an independent) Jeffreys prior for the concentration parameter, κ.

Each ODF in the UARS class is completely determined by the angular density $C(\cdot|\kappa)$. If $\lim_{r\to 0} \frac{C(r|\kappa)}{1-\cos r}$ is not finite, the ODF (1) is unbounded at $\mathbf{o} = \mathbf{S}$ and the corresponding model is non-regular. The estimators of parameters $\mathbf{S}$ and κ exhibit different asymptotic (as the sample size $n \to \infty$) behavior in non-regular models than in regular cases. So based on the forms of the angular densities $C(r|\kappa)$, we organize our discussion of the UARS models by first considering regular cases (rotational normal, Bunge, Matrix Fisher, de la Vallée Poussin (i.e. Cayley), and Lorentzian distributions) and then non-regular cases (vM-UARS, wMB-UARS and wN-UARS distributions). We provide expressions for the angular densities, and then we identify corresponding Jeffreys priors for concentration parameters.

2.1 Regular Cases

For these distributions, $\lim_{r\to 0} \frac{C(r|\kappa)}{1-\cos r}$ is finite. We use the same notation, κ, for the concentration parameters for all regular distributions. Except for the Lorentzian case, those distributions are essentially identical for large κ.

2.1.1 Rotational Normal Angular Distribution

The density for the rotational normal distribution's angular distribution is

$$C_{Normal}(r|\kappa) = \frac{1-\cos r}{2\pi}\sum_{m=0}^{\infty}(2m+1)\exp[-m(m+1)/(2\kappa^2)]\frac{\sin[(m+1/2)r]}{\sin(r/2)};$$

(Matthhies, 1988; Savjolova, 1985). To be consistent with the discussion of the Jeffreys prior for the wMB distribution introduced in Yu et al. (2012), we consider the corresponding Jeffreys prior for the spread parameter $\eta = -\log\kappa$ which has density

$$J(\eta) = \exp(-\eta)\sqrt{\mathcal{I}(\exp(-\eta))} \quad \eta \in (-\infty, \infty) \tag{2}$$

with

$$\begin{aligned}
\mathcal{I}(\kappa) &= -\,\mathrm{E}\left(\frac{d^2}{d\kappa^2}\log(C_{Normal}(r|\kappa))\right) \\
&= \frac{1}{\kappa^6}\int_{-\pi}^{\pi}\frac{\left(\sum_{m=0}^{\infty} m(m+1)f(r|m,\kappa)\right)^2}{\sum_{m=0}^{\infty} f(r|m,\kappa)}dr \\
&\quad -\frac{1}{\kappa^6}\int_{-\pi}^{\pi}\sum_{m=0}^{\infty}[m^2(m+1)^2 - 3m(m+1)\kappa^2]f(r|m,\kappa)dr
\end{aligned}$$

where $f(r|m,\kappa) = (2m+1)\exp[-m(m+1)/(2\kappa^2)]\frac{\sin[(m+1/2)r]}{\sin(r/2)}$. As $\eta \to \infty$, $J(\eta) \to 0$ and as $\eta \to -\infty$, $J(\eta) \to \sqrt{6}$. The Jeffreys prior above does not have a closed form, but can be computed numerically. We use $J(\eta) \approx \sqrt{6}$ when $\eta < -2$, $J(\eta) \approx 0$ when $\eta > 2$ and, for $-2 \le \eta \le 2$, we fit a cubic spline to approximate $J(\eta)$ after calculating the density at grid points $-2 + 4/1000 \cdot i$, $i = 0, 1, \cdots, 1000$.

2.1.2 Bunge Angular Distribution

The density for the Bunge angular distribution is

$$C_{Bunge}(r|\kappa) = \frac{1-\cos r}{2\pi} N(\kappa) \exp[-\kappa^2 r^2/2];$$

for a normalizing constant $N(\kappa)$ (Bunge,1982). The corresponding Jeffreys prior for the spread parameter $\eta = -\log \kappa$ has density (2) with

$$\begin{aligned} \mathcal{I}(\kappa) &= -\mathrm{E}\left(\frac{d^2}{d\kappa^2}\log(C_{Bunge}(r|\kappa))\right) \\ &= 2.46595 - \frac{d^2 N(\kappa)}{d\kappa^2} \end{aligned}$$

As $\eta \to \infty, J(\eta) \to 0$ and as $\eta \to -\infty, J(\eta) \to \sqrt{6}$. We use $J(\eta) \approx \sqrt{6}$ when $\eta < -2$, $J(\eta) \approx 0$ when $\eta > 3$ and, for $-2 \leq \eta \leq 3$, we fit a cubic spline to approximate $J(\eta)$ after calculating the density at grid points $-2 + 5/1000 \cdot i$, $i = 0, 1, \cdots, 1000$.

2.1.3 de la Vallée Poussin Angular Distribution

The density for the de la Vallée Poussin angular distribution is

$$C_{Poussin}(r|\kappa) = \frac{1-\cos r}{2\pi} \frac{B(3/2, 1/2)}{B(3/2, 2\kappa^2 + 1/2)} \cos^{4\kappa^2}(r/2);$$

(Schaeben, 1997). León et al. (2006) later derived the same distribution, calling it the Cayley distribution and providing an equivalent form for the

density,

$$C_{Cayley}(r|\kappa) = \frac{1-\cos r}{2\pi}\frac{\sqrt{\pi}\Gamma(2\kappa^2+2)(1+\cos r)^{2\kappa^2}}{2^{2\kappa^2}\Gamma(2\kappa^2+1/2)}.$$

The corresponding Jeffreys prior for the spread parameter $\eta = -\log\kappa$ has density (2) with

$$\begin{aligned}\mathcal{I}(\kappa) &= -\,\mathrm{E}\left(\frac{d^2}{d\kappa^2}\log(C_{Poussin}(r|\kappa))\right)\\ &= 2.21184 + \frac{6-30\kappa^2-72\kappa^4}{(2\kappa^2+1/2)^2(2\kappa^2+2)^2}\\ &\quad + \sum_{n=1}^{\infty}\frac{72\kappa^4+30\kappa^2+24\kappa^2 n-6n^2-15n-6}{(2\kappa^2+1/2+n)^2(2\kappa^2+2+n)^2}\end{aligned}$$

As $\eta\to\infty, J(\eta)\to 0$ and as $\eta\to-\infty, J(\eta)\to\sqrt{6}$. We use $J(\eta)\approx\sqrt{6}$ when $\eta<-2$, $J(\eta)\approx 0$ when $\eta>4$ and, for $-2\le\eta\le 4$, we fit a cubic spline to approximate $J(\eta)$ after calculating the density at grid points $-2+6/1000\cdot i$, $i=0,1,\cdots,1000$.

2.1.4 Lorentzian Angular Distribution

The density for the Lorentzian angular distribution is

$$C_{Lorentzian}(r|\kappa) = \frac{1-\cos r}{2\pi}(1+\lambda)\frac{(1+2\lambda)^2+4\lambda(\lambda+1)\cos^2(r/2)}{[(1+2\lambda)^2-4\lambda(\lambda+1)\cos^2(r/2)]^2};$$

(Matthies, 1982). Setting $\lambda = \kappa/2 - 0.5 + 2/(\kappa+2)^2$ puts the Lorentzian distribution on roughly the same scale as the others, but the large κ Lorentzian shape differs from the others. The corresponding Jeffreys prior for the spread

parameter $\eta = -\log\kappa$ has density (2) with

$$\begin{aligned}\mathcal{I}(\kappa) &= -\,\mathrm{E}\left(\frac{d^2}{d\kappa^2}\log(C_{Lorentzian}(r|\kappa))\right)\\ &= \frac{12}{(\kappa+2)^4}\int_{-\pi}^{\pi} C'_{Lorentzian}(r|\kappa)dr + [\frac{1}{2} - \frac{4}{(\kappa+2)^3}]^2\int_{-\pi}^{\pi} C''_{Lorentzian}(r|\kappa)dr\\ &\quad -[0.5 - 4(\kappa+2)^{-3}]^2\int_{-\pi}^{\pi}\frac{[C'_{Lorentzian}(r|\kappa)]^2}{C_{Lorentzian}(r|\kappa)}dr\end{aligned}$$

As $\eta \to \infty, J(\eta) \to 0$ and as $\eta \to -\infty, J(\eta) \to 1$. We use $J(\eta) \approx 1$ when $\eta < -2$, $J(\eta) \approx 0$ when $\eta > 8$ and, for $-2 \le \eta \le 8$, we fit a cubic spline to approximate $J(\eta)$ after calculating the density at grid points $-2 + 10/1000 \cdot i$, $i = 0, 1, \cdots, 1000$.

2.1.5 Matrix Fisher Angular Distribution

Bingham et al. (2010) have treated the Matrix Fisher (MF) distribution. Here, to be consistent with the parameterizations of the other regular distributions for large κ, we reparameterize its density as

$$C_{MF}(r|\kappa) = \frac{1-\cos r}{2\pi}\frac{\exp(\kappa^2\cos r)}{I_0(\kappa^2) - I_1(\kappa^2)}$$

where I_i denotes the modified Bessel function of order i. The corresponding Jeffreys prior for the spread parameter $\eta = -\log\kappa$ has density (2) with

$$\begin{aligned}\mathcal{I}(\kappa) &= -\,\mathrm{E}\left(\frac{d^2}{d\kappa^2}\log(C_{MF}(r|\kappa))\right)\\ &= -2\,\mathrm{E}(\cos(r)) + \frac{2I_0^2(\kappa^2) + (4 - 6/\kappa^2)I_0(\kappa^2)I_1(\kappa^2) + (2/\kappa^2 - 6)I_1^2(\kappa^2)}{(I_0(\kappa^2) - I_1(\kappa^2))^2}\end{aligned}$$

As $\eta \to \infty, J(\eta) \to 0$ and as $\eta \to -\infty, J(\eta) \to \sqrt{6}$.

2.2 Non-regular Cases

For these angular distributions, $\lim_{r\to 0} \frac{C(r|\kappa)}{1-\cos r}$ is infinite and the UARS ODF (1) has a singularity at $\mathbf{o} = \mathbf{S}$.

2.2.1 Wrapped Normal Angular Distribution

Unlike the angular densities for regular UARS models, the wN angular density is unimodal on $(-\pi, \pi]$, and is

$$C_{wNM}(r|\kappa) = \frac{\kappa}{\sqrt{2\pi}} \sum_{m=-\infty}^{\infty} \exp(-(2m\pi - r)^2\kappa^2/2), \quad r \in (-\pi, \pi]$$

The corresponding Jeffreys prior for the spread parameter $\eta = -\log\kappa$ has density

$$J(\eta) = \exp(-\eta)\sqrt{\mathcal{I}(\exp(-\eta))} \quad \eta \in (-\infty, \infty)$$

with

$$\begin{aligned} \mathcal{I}(\kappa) &= -\mathrm{E}\left(\frac{d^2}{d\kappa^2}\log(C_{wNM}(r|\kappa))\right) \\ &= -\frac{1}{\kappa^2} + \frac{\kappa^2}{\sqrt{2\pi}}\int_{-\pi}^{\pi} \frac{\left(\sum_{m=-\infty}^{\infty}(2m\pi - r)^2\exp(-\kappa^2(2m\pi - r)^2/2)\right)^2}{\sum_{m=-\infty}^{\infty}\exp(-\kappa^2(2m\pi - r)^2/2)}dr \end{aligned}$$

As $\eta \to \infty, J(\eta) \to 0$ and as $\eta \to -\infty, J(\eta) \to \sqrt{2}$. We use $J(\eta) \approx \sqrt{2}$ when $\eta < -0.5$, $J(\eta) \approx 0$ when $\eta > 2$ and, for $-0.5 \leq \eta \leq 2$, we fit a cubic spline to approximate $J(\eta)$ after calculating the density at grid points $-0.5+2.5/1000 \cdot i$, $i = 0, 1, \cdots, 1000$.

2.2.2 Von-Mises Angular Distribution

Bingham et al. (2009b) have used the von-Mises (vM) angular distribution for modeling rotations in texture analysis. For purposes of consistency with the wrapped normal angular density, we reparameterize its density as

$$C_{vM}(r|\kappa) = \frac{1 - \cos r}{2\pi} \frac{\exp(\kappa^2 \cos r)}{I_0(\kappa^2)}$$

where I_i denotes the modified Bessel function of order i. The corresponding Jeffreys prior for the spread parameter $\eta = -\log \kappa$ has density (2) with

$$\begin{aligned} \mathcal{I}(\kappa) &= -\,\mathrm{E}\left(\frac{d^2}{d\kappa^2} \log(C_{vM}(r|\kappa))\right) \\ &= -2\,\mathrm{E}(\cos(r)) + \frac{4\kappa^2 I_0^2(\kappa^2) - 2I_0(\kappa^2)I_1(\kappa^2) - 4\kappa^2 I_1^2(\kappa^2)}{I_0^2(\kappa^2)} \end{aligned}$$

As $\eta \to \infty, J(\eta) \to 0$ and as $\eta \to -\infty, J(\eta) \to \sqrt{2}$.

2.2.3 Wrapped Maxwell-Boltzman Angular Distribution

Yu et al.(2012) have introduced the wrapped Maxwell-Boltzman (wMB) angular distribution, and here it is worthwhile to reiterate its form

$$C_{wMB}(r|\kappa) = \frac{\kappa^3}{\sqrt{2\pi}} \sum_{m=-\infty}^{\infty} (2m\pi - r)^2 \exp(-\kappa^2(2m\pi - r)^2/2)$$

and the corresponding Jeffereys prior for the spread parameter $\eta = -\log \kappa$ which has a density (2) with

$$\begin{aligned} \mathcal{I}(\kappa) &= -\mathrm{E}\left(\frac{d^2}{d\kappa^2}\log(C_{wMB}(r|\kappa))\right) \\ &= -\frac{9}{\kappa^2} + \frac{\kappa^5}{\sqrt{2\pi}} \int_{-\pi}^{\pi} \frac{\left(\sum_{m=-\infty}^{\infty}(2m\pi - r)^4 \exp(-\kappa^2(2m\pi - r)^2/2)\right)^2}{\sum_{m=-\infty}^{\infty}(2m\pi - r)^2 \exp(-\kappa^2(2m\pi - r)^2/2)} dr. \end{aligned}$$

As $\eta \to \infty, J(\eta) \to 0$ and as $\eta \to -\infty, J(\eta) \to \sqrt{6}$.

2.3 Visual Summary of Models and Jeffreys Priors

For visual comparison purposes, plots of 8 sets of angular densities and the corresponding Jeffereys prior densities (here we rescale the Jeffereys prior densities such that they converge to 1 as η goes to $-\infty$) are given in Figures 1 and 2.

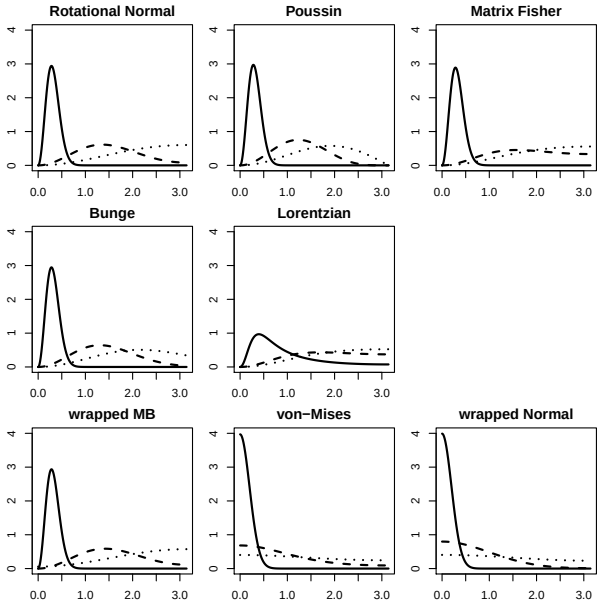

Figure 1: Absolute angular densities (i.e., densities for $|r|$) when $\kappa = 0.5(\text{dotted}), 1(\text{dashed}), 5(\text{solid})$.

3 One-sample Bayes Inference

We consider one-sample Bayes inference using the improper Jeffreys priors for concentration parameters and uniform distributions for central orientation parameters. For n observations $\mathbf{o}_i$, $i = 1, ..., n$ from some UARS density (1), the corresponding likelihood function for $(\mathbf{S}, \eta)$ is

$$L(\mathbf{S}, \eta) \propto \frac{\prod_{i=1}^{n} C(\arccos[2^{-1}(tr(\mathbf{S}^T\mathbf{o}_i) - 1)]| \exp(-\eta))}{\prod_{i=1}^{n}(3 - tr(\mathbf{S}^T\mathbf{o}_i))}.$$

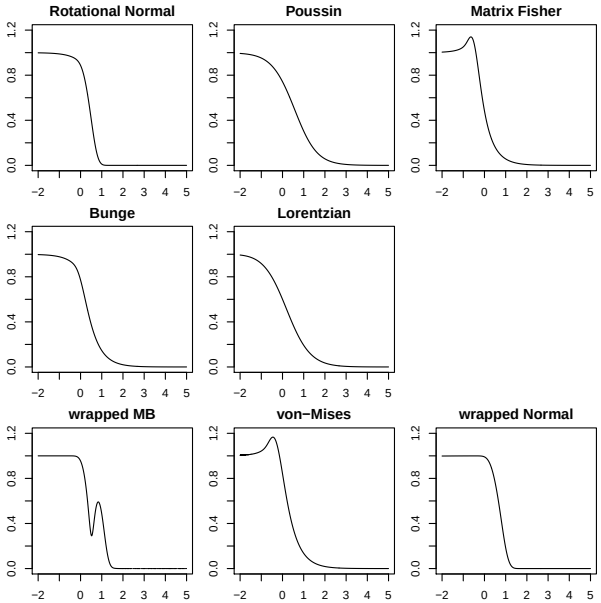

Figure 2: Rescaled Jeffereys prior densities of $\eta = -\log\kappa$ for all 8 angular distributions.

Multiplying by priors $p(\mathbf{S})$ and $J(\eta)$ gives a posterior density for $(\mathbf{S}, \eta)$ proportional to

$$\left(\frac{\prod_{i=1}^{n} C_{wMB}(\arccos[2^{-1}(tr(\mathbf{S}^T\mathbf{o}_i) - 1)]|\exp(-\eta))}{\prod_{i=1}^{n}(3 - tr(\mathbf{S}^T\mathbf{o}_i))} \right) J(\eta).$$

We may sample a sequence of pairs, $(\mathbf{S}^j, \eta^j)$, from the posterior distribution using the basic Metropolis-Hastings-within-Gibbs (MHG) algorithm of Bingham et al. (2009b) as follows. With observations $\mathbf{o}_1, ..., \mathbf{o}_n \in SO(3)$ and the starting values $\mathbf{S}^0, \eta^0$:

1. Generate $\mathbf{S}^{j*}$ from the Matrix Fisher rotational distribution with location parameter $\mathbf{S}^{j-1}$ and concentration parameter ρ. (Here ρ is a tuning parameter.)

2. Compute $r_j^1 = \frac{h(\mathbf{S}^{j^*}, \eta^{j-1})}{h(\mathbf{S}^{j-1}, \eta^{j-1})}$ and generate $W_j^1 \sim$ Bernoulli$(\min(1, r_j^1))$. Take $\mathbf{S}^j = W_j^1 \mathbf{S}^{j^*} + (1 - W_j^1)\mathbf{S}^{j-1}$.

3. Generate $\eta^{j^*} \sim N(\eta^{j-1}, \gamma^2)$. (Here γ is a tuning parameter.)

4. Compute $r_j^2 = \frac{h(\mathbf{S}^j, \eta^{j^*})}{h(\mathbf{S}^j, \eta^{j-1})}$ and generate $W_j^2 \sim$ Bernoulli$(\min(1, r_j^2))$. Take $\eta^j = W_j^2 \eta^{j^*} + (1 - W_j^2)\eta^{j-1}$.

With the simulated $\mathbf{S}$ and η, we can create approximately 95% credible regions for the parameters. One advantage of the Bayes method is that we can make a geometrically interpretable credible region for the parameter $\mathbf{S}$ as follows. First, we define a Bayes point estimator $\mathbf{S}_B$ as the minimizer of $tr(\mathbf{S}_B^T \bar{\mathbf{S}})$ based on the average $\bar{\mathbf{S}}$ of 100000 orientations $\mathbf{S}_i, i = 1, \ldots, 100000$ simulated from the posterior. Then we obtain a set of cones around axes representing $\mathbf{S}_B$ with angle a as the boundary of a 95% credible region for $\mathbf{S}$ (where where a is the 95th percentile of $\{a_1, \ldots, a_{100000}\}$ and each a_j represents the maximum arccosine value (between 0 and π) of the diagonal elements of $\mathbf{S}_B^T \mathbf{S}_j$). Details of the method and graphical interpretations can be found in Bingham et al. (2009b), Bingham et al. (2010), and Yu et al. (2012). The value of the angle between the center and edge of the cones can be used as the size of the credible region for $\mathbf{S}$.

In the next section, we provide a simulation study using the above algorithm to perform one-sample Bayes analyses (for the UARS distributions with Bayes methods not yet treated in the literature) for several choices of η and n. We then summarize the frequentist coverage probabilities and sizes of credible regions obtained from the Bayes methods and thereby establish the

effectiveness of the non-informative Bayes methods.

4 Simulation Results

To simulate test data sets from the UARS distributions, we chose the values of the parameter η of $-1.844, -1.151, -0.347, 0, 0.5, 1$ and sample sizes were $n = 10, 30, 100, 300, 1000$. Here we held the parameter $\mathbf{S}$ constant at $\mathbf{I}_{3\times 3}$ as the choice of $\mathbf{S}$ is irrelevant (Bingham et al. 2009a).

For each UARS distribution with one combination of sample size n and parameter η, we simulated 4000 data sets, each consisting of a random sample of n observations. For each data set, we generated 100000 samples from the posterior distribution using the MHG algorithm after a 25000 iteration burn-in period. (The starting values for $\mathbf{S}^0$ and η^0 in the simulation study were chosen to be the true parameters, as we determined that the choice of starting values did not affect posterior simulation results with a 25000 iteration burn-in period.) The tuning parameters ρ and γ were chosen to keep the Metropolis-Hastings jumping rates between 30% and 40% and are given in Appendix A.

Then we computed 95% credible regions for the two parameters for each set of simulated data. For parameter η, both equal-tail (ET) and shortest length (SL) intervals were obtained. For the parameter $\mathbf{S}$, we used the cone-based credible sets provided by Bingham et al. (2009b) as described above. For the 95% credible regions for $\mathbf{S}$ and η, we found coverage rates for $\mathbf{S}$ and η (determining the proportion of simulation runs for which credible regions

contained the true values). And we also considered median sizes for the 4000 regions for $\mathbf{S}$ and η. Results are given in Appendices B and C. For both $\mathbf{S}$ and η, the frequentist coverage rates of Bayes regions for each UARS distribution are consistent with their credible levels, and as sample size increases, the coverage rates converge more or less exactly to the nominal ones. This indicates that the Bayes approach is effective across the UARS class for obtaining good frequentist coverage accuracy.

In the meantime, for all combinations (n, η), the equal-tail and shortest-length methods produce similar 95% intervals for η. Also, for fixed η, as sample size n increases, the intervals become narrower. For fixed n, the median width of interval for η is monotone decreasing in η. (This is true in the present new simulations. Interestingly, strict monotonicity doesn't hold in the wMB UARS case. See Yu, et al. (2012) for details.)

As we said before, the size of a cone-based credible region for $\mathbf{S}$ is characterized by the angle defining the conic region. For fixed η, the median angle decreases as n increases. The empirical convergence rate (found by regressing the log of median angle over the log of n for $n = 100, 300, 1000$) is approximately $O(1/\sqrt{n})$ for regular cases, consistent with the smoothness of their likelihood functions, and approximately $O(1/n)$ for the wN-UARS distribution, consistent with the fact that its likelihood function has singularities. (For details of the rate issue for Bayes methods in non-regular models of this type, see Nordman et al. 2009.)

We also note that, for the regular cases, the Bayes results here essentially

match those found by Bingham et.al. (2010) for the (regular) symmetric Matrix Fisher distribution. For non-regular cases, simulations in Bingham et al. (2009b) and Yu et al. (2012) for the (non-regular) vM-UARS and wMB-UARS models agree with findings here as well.

5 Discussion

Between this paper and the existing literature (Bingham et al. 2009b, Bingham et al. 2010, and Yu et al. 2012), we have established a complete one-sample non-informative Bayes methodology which is reasonable and effective for 8 parametric UARS symmetric distributions for 3-D rotations, 5 that are regular statistical models and 3 that are non-regular models. One can investigate which UARS distribution best describes an orientation data set using probability plots of estimated absolute misorientation angles for each fitted distribution. See Bingham et al. (2009a) for details. Because the UARS class has wide usefulness, our next step will be the development of an `R` package implementing non-informative Bayes methods for the UARS class.

Appendix

A. Tuning Parameters

Table 1: Values of tuning parameters ρ and γ for MCMC.

	Normal		Bunge		de la Vallée Poussin		Lorentzian		wrapped Normal	
(n, η)	ρ	γ	ρ	γ	ρ	γ	ρ	γ	ρ	γ
$(10, 1)$	0.02	0.65	1.9	0.5	7.75	0.5	0.14	0.9	34.64	0.4
$(30, 1)$	16.12	0.65	20	0.5	20	0.5	4	0.5	77.46	0.25
$(100, 1)$	200	0.65	63.25	0.5	40	0.25	1.55	0.3	244.94	0.12
$(300, 1)$	316.22	0.65	126.49	0.5	100	0.2	13	0.2	774.6	0.05
$(1000, 1)$	1000	0.65	860.23	0.5	24.26	0.15	18.97	0.12	2236.07	0.02
$(10, 0.5)$	4.47	0.65	0.45	0.5	0.04	0.5	0.14	0.9	40	0.4
$(30, 0.5)$	27.75	0.5	1.26	0.45	2	0.5	1.26	0.45	63.25	0.25
$(100, 0.5)$	83.67	0.5	2	0.3	2	0.35	1	0.3	200	0.12
$(300, 0.5)$	77.46	0.5	2.24	0.2	3.16	0.2	10.95	0.15	346.41	0.05
$(1000, 0.5)$	632.45	0.5	54.83	0.1	17.32	0.05	15.49	0.12	2449.49	0.02
$(10, 0)$	2.45	0.4	1	0.6	0.1	0.5	0.04	0.8	17.32	0.4
$(30, 0)$	4	0.23	3.16	0.23	1.14	0.5	0.14	0.45	22.36	0.25
$(100, 0)$	10	0.13	4.9	0.13	2.45	0.35	1.41	0.3	24.49	0.15
$(300, 0)$	14.14	0.07	7.75	0.07	4	0.2	7.75	0.2	30	0.07
$(1000, 0)$	31.62	0.04	14.14	0.04	4	0.1	17.32	0.1	282.84	0.05
$(10, -0.347)$	4.47	0.4	2.45	0.5	1.9	0.4	0.04	0.8	7.75	0.4
$(30, -0.347)$	10	0.23	4.9	0.23	1.9	0.4	1.41	0.5	31.62	0.2
$(100, -0.347)$	12.65	0.13	10	0.13	6.32	0.13	10	0.3	34.64	0.15
$(300, -0.347)$	14.14	0.07	17.32	0.07	10	0.07	4.9	0.1	40	0.07
$(1000, -0.347)$	44.72	0.04	31.62	0.04	20	0.04	11.83	0.05	141.42	0.05
$(10, -1.151)$	10	0.4	7.75	0.4	6.32	0.4	2.45	0.5	4.47	0.4
$(30, -1.151)$	10	0.23	14.14	0.23	12.65	0.23	6.32	0.25	20	0.3
$(100, -1.151)$	20	0.13	26.46	0.13	24.49	0.13	8.94	0.15	44.72	0.3
$(300, -1.151)$	40	0.07	40	0.07	40	0.07	14.14	0.08	50	0.07
$(1000, -1.151)$	70.71	0.04	77.46	0.04	77.46	0.04	30	0.05	173.20	0.05
$(10, -1.844)$	10	0.4	14.14	0.4	14.14	0.4	4.47	0.4	6.32	0.4
$(30, -1.844)$	20	0.23	30	0.23	28.28	0.23	7.75	0.25	44.72	0.4
$(100, -1.844)$	28.28	0.13	48.99	0.13	54.77	0.13	17.32	0.15	44.72	0.3
$(300, -1.844)$	63.25	0.07	89.44	0.07	77.46	0.07	24.49	0.08	54.74	0.07
$(1000, -1.844)$	100	0.04	154.92	0.07	141.42	0.04	54.77	0.04	223.61	0.05

B. Coverage Rates

C. Median Widths of Credible Regions

Table 2: Coverage rates (%) for $\mathbf{S}$ and η using 95% Bayes credible regions. (Credible regions for η characterized here are ET intervals.)

	Normal		Bunge		de la Vallée Poussin		Lorentzian		wrapped Normal	
(n, η)	$\mathbf{S}$	η	$\mathbf{S}$	η	$\mathbf{S}$	η	$\mathbf{S}$	η	$\mathbf{S}$	η
(10,1)	94.4	94.8	97.0	96.1	94.2	98.3	92.1	93.6	93.4	94.0
(30,1)	96.0	95.8	96.0	95.7	98.2	94.8	93.3	93.2	95.0	95.8
(100,1)	94.8	95.6	95.5	94.8	96.5	94.8	93.5	94.0	94.8	95.6
(300,1)	95.6	95.2	95.1	95.3	96.0	94.8	94.3	94.5	94.6	95.1
(1000,1)	95.2	95.0	95.1	95.2	95.5	94.9	94.5	94.7	94.9	95.0
$(10, 0.5)$	96.1	96.5	97.2	96.3	94.1	98.8	94.6	92.7	96.7	96.3
$(30, 0.5)$	98.0	96.7	95.0	96.1	95.6	97.8	95.5	93.4	97.0	95.7
$(100, 0.5)$	96.3	96.5	94.9	95.3	94.8	96.7	94.8	94.4	96.3	95.1
$(300, 0.5)$	95.7	95.3	95.1	94.9	94.8	94.6	95.3	95.5	94.5	94.8
$(1000, 0.5)$	95.1	95.1	95.1	95.1	95.2	94.9	95.1	95.4	95.1	95.2
$(10, 0)$	97.5	97.1	95.5	96.4	94.7	95.0	93.3	92.6	93.7	94.3
$(30, 0)$	95.0	95.9	96.0	96.7	93.7	94.3	94.5	95.1	93.9	94.2
$(100, 0)$	95.7	94.9	95.7	95.8	97.2	95.1	95.6	96.7	96.7	96.6
$(300, 0)$	95.5	94.9	95.1	95.5	95.7	96.5	95.1	95.8	95.3	94.7
$(1000, 0)$	95.3	95.0	95.3	95.3	94.8	95.1	95.4	95.1	95.0	95.1
$(10, -0.347)$	94.1	94.0	95.6	95.8	93.1	97.1	95.5	96.7	93.9	93.5
$(30, -0.347)$	98.0	97.8	93.0	93.9	97.4	97.0	95.9	96.6	94.0	94.8
$(100, -0.347)$	96.1	95.3	95.1	94.8	93.8	96.1	95.9	95.3	96.1	95.7
$(300, -0.347)$	95.3	95.5	95.3	94.8	95.1	96.3	95.0	95.6	95.4	94.9
$(1000, -0.347)$	95.1	95.4	95.1	95.0	95.2	94.9	95.0	94.9	94.9	95.1
$(10, -1.151)$	94.5	94.5	95.5	95.5	94.2	94.9	95.6	97.2	94.5	94.5
$(30, -1.151)$	93.0	93.3	95.0	95.7	94.9	94.7	93.6	94.8	93.8	94.4
$(100, -1.151)$	94.6	94.7	94.6	95.3	94.9	94.5	94.9	95.2	94.1	93.9
$(300, -1.151)$	94.9	94.8	94.9	95.0	95.0	95.2	95.5	95.1	94.7	95.6
$(1000, -1.151)$	94.9	95.0	95.0	95.0	95.0	95.2	94.9	94.9	94.8	95.2
$(10, -1.844)$	95.2	96.1	93.2	93.5	93.1	93.4	93.7	94.3	95.2	95.1
$(30, -1.844)$	93.2	93.0	97.5	96.9	94.8	94.6	94.0	94.6	94.2	95.0
$(100, -1.844)$	94.6	94.8	96.2	96.2	94.9	95.1	95.2	94.2	95.6	95.5
$(300, -1.844)$	95.0	95.2	95.1	94.9	94.6	94.8	95.2	94.9	95.0	94.9
$(1000, -1.844)$	94.9	95.0	95.0	94.9	95.0	95.1	95.3	94.7	94.9	94.9

Table 3: Median widths of 95% Bayes credible intervals for η for both equal-tail (ET) and shortest-length (SL) intervals.

	Normal		Bunge		de la Vallée Poussin		Lorentzian		wrapped Normal	
(n, η)	ET Width	SL Width	ET Width	SL Width	ET Width	SL Width	ET Width	SL Width	ET Width	SL Width
(10,1)	1.9868	1.956	1.9789	1.7481	1.9091	1.7097	1.9812	1.7646	0.5126	0.5085
(30,1)	0.6956	0.6804	0.8877	0.7650	1.7395	1.5040	0.9434	0.9079	0.288	0.2791
(100,1)	0.5826	0.5644	0.5514	0.4483	1.2559	1.0711	0.5101	0.5080	0.1433	0.1294
(300,1)	0.3678	0.3592	0.4051	0.3154	1.2535	1.0579	0.4234	0.4211	0.0723	0.0627
(1000,1)	0.1247	0.1212	0.3521	0.2754	0.5309	0.4221	0.3521	0.2754	0.0282	0.0237
$(10, 0.5)$	0.8218	0.8099	1.5587	1.3685	1.3117	1.2773	1.7774	1.5465	0.5234	0.5192
$(30, 0.5)$	0.6156	0.6078	0.8385	0.8016	0.7656	0.7482	0.8218	0.8044	0.2923	0.2907
$(100, 0.5)$	0.3810	0.3772	0.4899	0.4853	0.3395	0.3040	0.3997	0.3981	0.1516	0.1390
$(300, 0.5)$	0.2781	0.2764	0.3142	0.2942	0.3087	0.2878	0.2577	0.2526	0.0787	0.692
$(1000, 0.5)$	0.1098	0.1093	0.1626	0.1691	0.1672	0.1667	0.1847	0.1819	0.0319	0.0267
$(10, 0)$	0.7967	0.7670	1.5088	1.3415	1.1656	1.1547	1.7706	1.5299	0.5221	0.5207
$(30, 0)$	0.4321	0.3980	0.8126	0.7144	0.7941	0.785	0.8012	0.7790	0.29	0.2893
$(100, 0)$	0.1728	0.1719	0.1796	0.1788	0.1793	0.1786	0.4245	0.4233	0.1615	0.1604
$(300, 0)$	0.1005	0.0995	0.1005	0.0996	0.1017	0.0985	0.4186	0.4169	0.0933	0.0932
$(1000, 0)$	0.0535	0.0532	0.0535	0.0533	0.0536	0.0534	0.1583	0.1522	0.0502	0.0499
$(10, -0.347)$	0.5620	0.5530	0.5636	0.5548	0.5664	0.5549	1.9198	1.6785	0.5274	0.5247
$(30, -0.347)$	0.2986	0.2978	0.2990	0.2974	0.4327	0.3831	1.1575	1.0266	0.2938	0.2930
$(100, -0.347)$	0.1633	0.1629	0.1660	0.1648	0.1632	0.1628	0.9006	0.8974	0.1637	0.1635
$(300, -0.347)$	0.0932	0.0924	0.0933	0.0928	0.0932	0.0924	0.1280	0.1278	0.0920	0.0919
$(1000, -0.347)$	0.0516	0.0515	0.0518	0.0517	0.0516	0.0515	0.0619	0.0617	0.0526	0.0523
$(10, -1.151)$	0.5436	0.5389	0.5431	0.5387	0.5421	0.5372	1.8427	1.2750	0.5280	0.5268
$(30, -1.151)$	0.2985	0.2977	0.2985	0.2967	0.2980	0.2963	1.3011	1.2994	0.2981	0.2964
$(100, -1.151)$	0.1632	0.1627	0.1631	0.1630	0.1630	0.1625	0.1647	0.1626	0.1631	0.1628
$(300, -1.151)$	0.0923	0.0921	0.0924	0.0922	0.0923	0.0921	0.0937	0.0933	0.0933	0.0926
$(1000, -1.151)$	0.0507	0.0505	0.0509	0.0506	0.0506	0.0503	0.0514	0.0511	0.0543	0.0543
$(10, -1.844)$	0.5423	0.5379	0.5427	0.5379	0.5404	0.5357	0.5399	0.5359	0.5244	0.5232
$(30, -1.844)$	0.2981	0.2972	0.2985	0.2969	0.2976	0.2946	0.2985	0.2970	0.2993	0.2989
$(100, -1.844)$	0.1625	0.1620	0.1632	0.1623	0.1621	0.1615	0.1641	0.1632	0.1625	0.1623
$(300, -1.844)$	0.0923	0.0920	0.0921	0.0919	0.0923	0.0920	0.0931	0.0921	0.0926	0.0923
$(1000, -1.844)$	0.0504	0.0502	0.0507	0.0505	0.0505	0.0505	0.0503	0.0502	0.0560	0.0555

Table 4: Median cone angles of 95% Bayes credible sets for **S** and the apparent (moderate sample size) convergence rates of the median angles for fixed η.

	Normal		Bunge		de la Vallée Poussin		Lorentzian		wrapped Normal	
(n, η)	Angle	Rate	Angle	Rate	Angle	Rate	Angle	Rate	Angle	Rate
(10,1)	1.1309		1.1309		1.0771		1.5410		0.9254	
(30,1)	0.4097		0.3972		0.4052		0.5353		0.4052	
(100,1)	0.0343	$n^{-0.57}$	0.0327	$n^{-0.56}$	0.0395	$n^{-0.57}$	0.0514	$n^{-0.53}$	0.0266	$n^{-1.05}$
(300,1)	0.01623		0.01489		0.0258		0.0387		0.004	
(1000,1)	0.0091		0.0089		0.0108		0.0152		0.0023	
$(10, 0.5)$	1.5355		1.5825		1.5422		1.5465		0.1634	
$(30, 0.5)$	1.5206		1.5296		1.5358		1.5430		0.0565	
$(100, 0.5)$	1.4773	$n^{-0.50}$	1.5218	$n^{-0.50}$	1.5294	$n^{-0.53}$	0.5490	$n^{-0.52}$	0.0179	n^{-1}
$(300, 0.5)$	1.2459		1.2611		1.3221		0.250		0.0081	
$(1000, 0.5)$	0.4713		0.4888		0.4532		0.123		0.0018	
$(10, 0)$	1.3537		1.4198		1.5708		1.5466		0.2852	
$(30, 0)$	0.8694		1.0153		1.5535		1.5412		0.0862	
$(100, 0)$	0.3961	$n^{-0.50}$	0.4606	$n^{-0.52}$	0.5123	$n^{-0.50}$	0.5446	$n^{-0.54}$	0.0456	$n^{-1.11}$
$(300, 0)$	0.2312		0.2502		0.4593		0.2898		0.0099	
$(1000, 0)$	0.1246		0.1388		0.1633		0.1584		0.0035	
$(10, -0.347)$	0.7324		0.7508		0.7779		1.5345		0.4299	
$(30, -0.347)$	0.4033		0.4105		0.5708		1.4652		0.083	
$(100, -0.347)$	0.2304	$n^{-0.52}$	0.2302	$n^{-0.51}$	0.4061	$n^{-0.54}$	0.3116	$n^{-0.50}$	0.0564	$n^{-1.07}$
$(300, -0.347)$	0.1249		0.1299		0.2098		0.1403		0.0086	
$(1000, -0.347)$	0.0694		0.0709		0.1172		0.0973		0.0047	
$(10, -1.151)$	0.2918		0.3004		0.5708		0.8312		0.6161	
$(30, -1.151)$	0.1633		0.1638		0.3031		0.4459		0.0448	
$(100, -1.151)$	0.0913	$n^{-0.52}$	0.0915	$n^{-0.51}$	0.0940	$n^{-0.51}$	0.2457	$n^{-0.51}$	0.0139	$n^{-1.1}$
$(300, -1.151)$	0.0481		0.0489		0.0471		0.1348		0.0048	
$(1000, -1.151)$	0.0274		0.0279		0.0289		0.0752		0.0011	
$(10, -1.844)$	0.1430		0.1444		0.5708		0.4606		0.5039	
$(30, -1.844)$	0.0799		0.0814		0.0796		0.0776		0.0480	
$(100, -1.844)$	0.0452	$n^{-0.51}$	0.0415	$n^{-0.49}$	0.0431	$n^{-0.49}$	0.0405	$n^{-0.50}$	0.015	$n^{-1.02}$
$(300, -1.844)$	0.0291		0.0243		0.0296		0.0380		0.0024	
$(1000, -1.844)$	0.0139		0.0134		0.0140		0.0129		0.0014	

References

Bingham, M.A., Nordman, D.J. and Vardeman, S.B. (2009a). Modeling and Inference for Measured Crystal Orientations and a Tractable Class of Symmetric Distributions for Rotations in Three Dimensions. *Journal of the American Statistical Association* **104**, 1385-1397.

Bingham, M.A., Vardeman, S.B. and Nordman, D.J. (2009b). Bayes One-

Sample and One-Way Random Effects Analyses for 3-D Orientations with Application to Materials Science. *Bayesian Analysis* **4**, 607-630.

Bingham, M.A., Nordman, D.J. and Vardeman, S.B. (2010). Finite-Sample Investigation of Likelihood and Bayes Inference for the Symmetric von Mises-Fisher Distribution. *Computational Statistics and Data Analysis* **54**, 1317-1327.

Bunge, H.J. (1982). *Texture Analysis in Materials Science*. Butterworth, London.

Chang, T. and Rivest, L.-P. (2001). M-Estimation for Location and Regression Parameters in Group Models: A Case Study Using Stiefel Manifolds. *The Annals of Statistics* **29**, 784-814.

Downs, T.D. (1972). Orientation Statistics. *Biometrika* **59**, 665-676.

Hielscher, R., Schaeben, H. and Siemes H. (2010). Orientation Distribution Within a Single Hematite Crystal. *Mathematical Geosciences* **42**, 359-375.

Jupp, P.E. and Mardia, K.V. (1979). Maximum Likelihood Estimators for the Matrix Von Mises-Fisher and Bingham Distributions. *Annals of Statistics* **7**, 599-606.

Khatri, C.G. and Mardia, K.V. (1977). The Von Mises-Fisher Matrix Distribution in Orientation Statistics. *Journal of The Royal Statististical Society Series B* **39**, 95-106.

León, C.A., Massé, J.-C. and Rivest L.-P. (2006). A Statistical Model for Random Rotations. *Journal of Multivariate Analysis* **97**, 412-430.

Matthies, S. (1982). Form Effects in the Description of the Orientation Distribution Function (ODF) of Texturized Materials by Model Components. *Physica Status Solidi (b)* **112**, 705-716.

Matthies, S., Muller, J. and Vinel, G.W. (1988). On the Normal Distribution in the Orientation Space. *Textures and Microstructures* **10**, 77-96.

Nordman, D.J., Vardeman, S.B. and Bingham, M.A. (2009). Uniformly Hyper-efficient Bayes Inference in a Class of Non-regular Problems. *The American Statistician* **63**, 234-238.

Oualkacha, K. and Rivest L.-P.(2008). A New Statistical Model for Random Unit Vectors. *Journal of Multivariate Analysis* **100**, 70-80.

Savyolova, T.I. (1985). Preface to *Novye Metody Issledovanija Tekstury Polikristalliĉeskich Materialov*. Metallurgija, Moscow.

Schaeben, H. (1997). The de la Vallée Poussin Standard Orientation Density Function. *Textures and Microstructures* **33**, 365-373.

Supplementary Material for online publication only

Click here to download Supplementary Material for online publication only: wMB_cor_Sinica.pdf